

## Transient variation in seismic wave speed points to fast fluid movement in the Earth's outer core

Ying Zhou <sup>1</sup> 

The solid inner core grows through crystallization of the liquid metallic outer core. This process releases latent heat as well as light elements, providing thermal and chemical buoyancy forces to drive the Earth's geodynamo. Here we investigate temporal changes in the liquid outer core by measuring travel times of core-penetrating SKS waves produced by pairs of large earthquakes at close hypocenters. While the majority of the measurements do not require a change in the outer core, we observe SKS waves that propagate through the upper half of the outer core in the low latitude Pacific travel about one second faster at the time when the second earthquake occurred, about 20 years after the first earthquake. This observation can be explained by 2–3% of density deficit, possibly associated with high-concentration light elements in localized transient flows in the outer core, with a flow speed in the order of 40 km/year.

<sup>1</sup>Department of Geosciences, Virginia Tech, Blacksburg, VA 24061, USA. ✉email: [yingz@vt.edu](mailto:yingz@vt.edu)

Observations of seismic wavespeed and density of the Earth's outer core suggest the composition of the bulk outer core is not pure iron but has a density deficit of about 5–10%<sup>1</sup>, indicating the existence of a considerable amount of light elements in the outer core, possibly including hydrogen, carbon, nitrogen, oxygen, sulfur, and silicon<sup>2,3</sup>. As the Earth cools, the crystallization of the liquid iron releases light elements and the solid inner core grows. The time scale of the iron solidification process and the associated convection (geodynamo) remain unclear. If the released light elements are concentrated locally, they may have a detectable impact on the local seismic wavespeed. Seismic waves produced by large earthquakes provide a direct sampling of the Earth's outer core. The speed at which the seismic wave propagates through the outer core can be used to constrain lateral heterogeneities in the outer core<sup>4,5</sup>.

In this study, we investigate possible temporal changes in seismic wavespeed in the liquid outer core on a decade time scale by measuring differential travel times of core-penetrating SKS waves produced by pairs of large earthquakes with close hypocenters. The SKS waves travel as shear waves in the mantle and as compressional waves in the outer core. If two earthquakes occur at the same hypocenter but in different decades, the travel times of the SKS waves can be used to determine possible property changes in the outer core as convection in the mantle is a much slower process, on a million-year time scale. This task is not straightforward because earthquakes may occur closely in space such that the SKS waves sample approximately the same region in the mantle and the outer core, but they do not occur at the exact same hypocenters, and their focal mechanisms may be similar but different. To overcome this limitation, we measure the arrival times of the SKS waves as well as reference waves including core diffracted waves (Pdiff and Sdiff) and surface-reflected mantle waves (PP and SS). If there is a property change in the outer core between the time the two earthquakes occurred, it will affect the relative arrival times between the SKS waves and their reference waves differently from a change in earthquake hypocenters.

We analyze the double differential arrival times between SKS waves and their reference waves generated by pairs of large earthquakes that occurred in different decades between 1990 and 2019. The analysis shows that the majority of the travel time measurements do not require a temporal change in the outer core at a decade time scale. The most striking observation was five anomalous SKS waves that travel faster through the outer core at the time when the second earthquake occurred, about 20 years after the first earthquake. The travel time anomalies can not be explained by earthquake hypocenter mislocations but suggest about a 1–1.5% increase in P-wavespeed in the outer core in localized regions with a lateral radius of about 800 km. If this temporal change in wavespeed was compositional, the wavespeed increase would indicate a 2–3% of density deficit, possibly associated with a high concentration of light elements (e.g., 1–2% more sulfur) in localized upward flows in the outer core. The process is probably transient with a time scale of a couple of decades or shorter.

## Results

**Anomalous SKS travel times.** In Fig. 1, we compare seismograms recorded at station COLA in Alaska from two earthquakes with close hypocenters in the Kermadec Islands region in the South Pacific Ocean. The first earthquake occurred in May 1997 and the second earthquake occurred in September 2018. Example original seismograms from the two earthquakes are plotted in Fig. S1. When any of the reference waves (Pdiff, Sdiff, PP, or SS) from the two earthquakes are aligned, the SKS wave from the second earthquake arrives about 1 s earlier than the SKS wave from the

first earthquake. This observation can not be explained by differences in earthquake hypocenter locations. For example, the 1-s advance time in  $\delta t_{\text{SKS}} - \delta t_{\text{Sdiff}}$  alone may be explained if the 2018 earthquake was about 0.3° farther away from the station, but  $\delta t_{\text{SKS}} - \delta t_{\text{Pdiff}}$  is relatively insensitive to distance change, and it will predict a small delay (0.14 s) in the SKS arrival when Pdiff waves are aligned. However, we observe 1.1 s of SKS advance time in  $\delta t_{\text{SKS}} - \delta t_{\text{Pdiff}}$ . In addition, a distance change of 0.3° will also predict a large (1.9 s) differential arrival time between PP and SS waves, but the observed differential travel time is very small (0.15 s). Similarly, a 10-km mislocation in earthquake depth may explain the one second advance in  $\delta t_{\text{SKS}} - \delta t_{\text{Pdiff}}$  alone, but  $\delta t_{\text{SKS}} - \delta t_{\text{Sdiff}}$  is relatively insensitive to focal depth change (0.1 s for 10 km). The observed  $\delta t_{\text{SKS}} - \delta t_{\text{Sdiff}}$  differential time is 1.05 s, an order of magnitude larger. Differences in focal mechanisms between the two earthquakes do not affect the travel times of these seismic phases (Fig. S2)

To investigate differential arrivals associated with uncertainties in earthquake hypocenter locations, we perform a grid search on earthquake hypocenter locations at a 1 km interval in a spherical region with a radius of 50 km, centered at the USGS PDE location of each earthquake. We calculate differential travel times between SKS waves and their reference waves associated with changes in earthquake hypocenter locations. The calculations show that most travel time measurement sets may be explained by potential mislocations of the earthquakes to within the maximum measurement uncertainty of 0.5 s (Methods). The most interesting finding is five anomalous measurement sets that could not be explained by possible earthquake mislocations, and, increasing the hypocenter search radius does not change the result. In all cases, the SKS waves travel faster through the outer core at the time of the second earthquake. They arrive earlier in seismograms when the reference waves from the two earthquakes are aligned. This indicates that P-wavespeed in the outer core in the regions sampled has changed (increased) when the second earthquake occurred.

In Fig. 2, we plot the smallest differential travel time change between SKS waves and their reference waves  $\delta t_{\text{SKS}} - \delta t_{\text{X}}$  (X: Pdiff, Sdiff, PP, SS) as a function of the latitude of the turning points of the SKS waves. The smallest differential travel time change does not carry significance in analysis but serves the purpose of illustrating the distribution of the dataset. Most of the smallest differential travel times are within the 1.5 standard deviations of the dataset. In addition, calculations show that those measurements can also be explained by possible hypocenter mislocations. The five anomalous measurement sets that can not be explained by location differences are plotted as solid blue dots. Four of the five measurements are from the same earthquake pair (P16), with the first earthquake in 1997 and the second one in 2018. Their PP and Pdiff seismograms show that their relative arrivals are small with  $\delta t_{\text{PP}} - \delta t_{\text{Pdiff}}$  less than 0.4 s (Fig. 3 and Fig. S1). This indicates that the epicenter distances of the two earthquakes are very close (with a difference less than 15 km). The fifth anomalous SKS wave that has a turning point latitude of 29.05°N was recorded at station CCM with the first earthquake in 1998 and the second earthquake in 2015.

The geographic distribution of the SKS ray paths in the outer core is plotted in Fig. 4. Most of the SKS waves in this study turn under the Pacific Ocean and East Asia, with several rays, traveling in the outer core under the Indian Ocean and the Arctic Ocean. The five anomalous SKS waves all turn in the low latitude Pacific Ocean. In addition, they all propagate in the upper half of the outer core. The ray paths in gray color are those measurements that may potentially be explained by possible event mislocations. It is possible that some of the SKS waves may also experience changes in core property but their impact on the SKS travel time

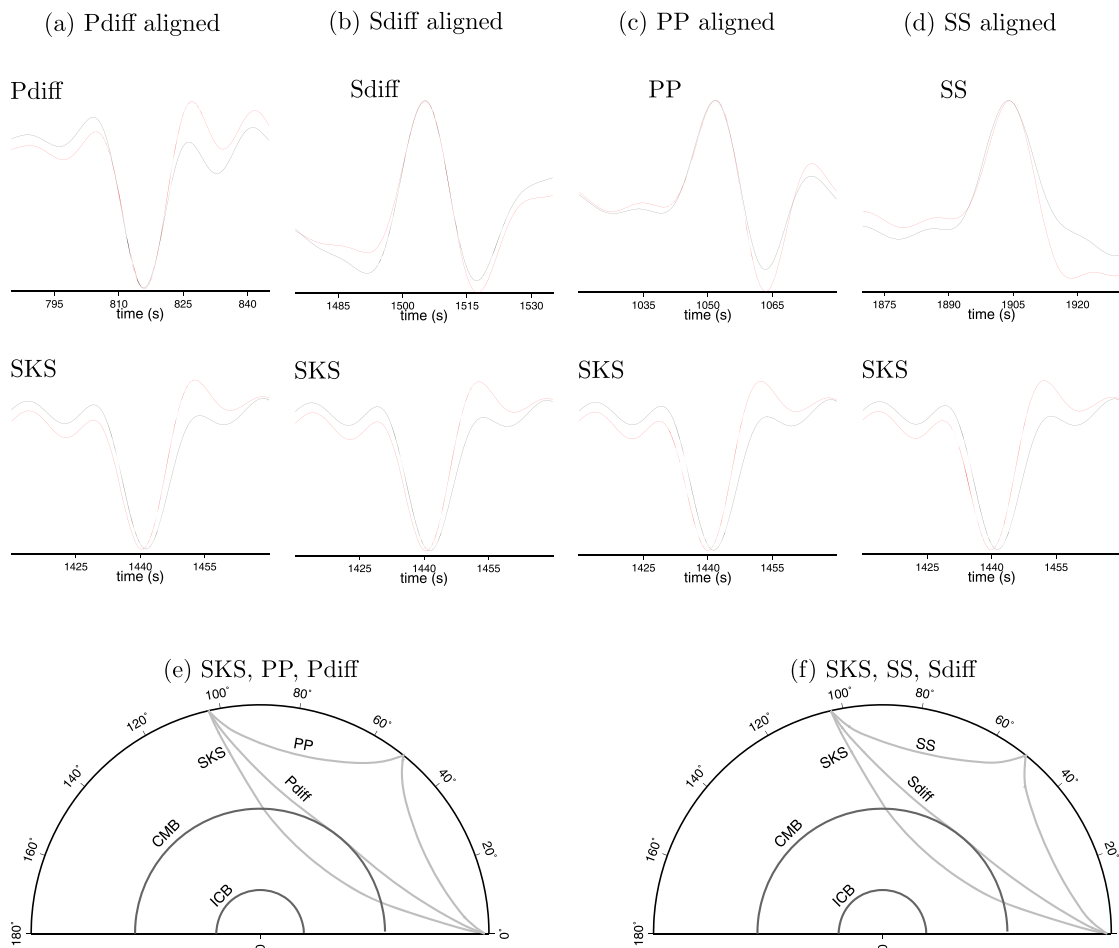


**Fig. 1** Faster SKS wave from the second earthquake when reference waves are aligned. **a–d** Displacement seismograms were recorded at station COLA for two earthquakes with close hypocenter locations, the first earthquake (black) occurred in 1997 and the second earthquake (red) occurred in 2018. The epicentral distance is  $\sim 99.4^\circ$ . The SKS wave in 2018 is about 1 s faster when the reference phases Pdiff, Sdiff, PP, or SS are aligned. The relative advance times are 1.1, 1.05, 1.5, and 1.35 seconds, respectively. The magnitudes and moment tensors of the two earthquakes are different and the amplitudes of the seismograms in 2018 have been multiplied by a constant factor for easier visual comparison only. Travel time measurements are made on the original seismograms. The cross-section view of the ray paths of the SKS, Pdiff, Sdiff, PP, and SS waves are plotted in **(e)** and **(f)** for reference.

does not significantly exceed measurement uncertainties associated with possible event mislocations. In Fig. 4, we show that large SKS advance time is only observed at a small number of seismic stations for the earthquake pair P16. This indicates that changes in the outer core occurred in localized regions only. While the two earthquake occurrences provide some constraints on the time scale of the process, it is unclear if the wavespeed change in the outer core occurs gradually over two decades or it reflects a more rapid process in a shorter time scale.

**Wave propagation modeling.** To constrain the size of the anomalous regions in the outer core associated with the observed SKS wavespeed change, we calculate synthetic seismograms in earth models with localized P-wavespeed perturbations in the outer core. In theory, a small-and-strong anomaly and a large-and-weak anomaly along the SKS ray path may produce the same amount of SKS advance time. However, their waveforms may be different due to wave diffraction. In Fig. 5, we calculate the finite-frequency sensitivities of SKS wave travel time and amplitude for measurements at station ULN using the adjoint method<sup>6</sup>. The turning point latitude of the SKS wave is  $9.96^\circ\text{N}$ . The sensitivities are calculated at a period of 30 s and the lateral size of the Fresnel zone at the turning depth is about  $12^\circ$  ( $\sim 800$  km). The travel time

has minimum sensitivity along the SKS ray path while the amplitude has maximum sensitivity along the ray path, as expected<sup>7,8</sup>. If the size of the anomalous region in the outer core is smaller than the size of the Fresnel zone, we may expect apparent wave diffraction effects. We calculate synthetic seismograms using the Spectral Element Method<sup>9</sup> for different sizes of anomalies in the outer core—a large anomaly that is about the same size as the Fresnel zone and a small anomaly that is smaller than the Fresnel zone. In Fig. 5, the blue dotted circle on the map view and blue dashed line in the cross-section view illustrate the size and location of a small axis-symmetrical anomaly with a lateral radius of  $6^\circ$  and a depth extent of 600 km. The P-wavespeed increase is 4% in this small anomaly. The red dotted circle and red dashed line illustrate the size and location of a large anomaly with a lateral radius of  $12^\circ$  ( $\sim 800$  km) and a depth extent of 800 km above the geometrical ray. P-wavespeed increase is 1.5% in the large anomaly.

Seismograms calculated with and without the wavespeed anomalies in the outer core are plotted in Fig. 6. The  $\sim 1.0$  s SKS advance time alone may be explained by either a small strong (4%) anomaly or a large weak (1.5%) anomaly. However, when the size of the anomaly is smaller than the Fresnel zone, strong diffraction occurs. The amplitude of the SKS wave becomes particularly smaller (defocusing) and the waveform becomes

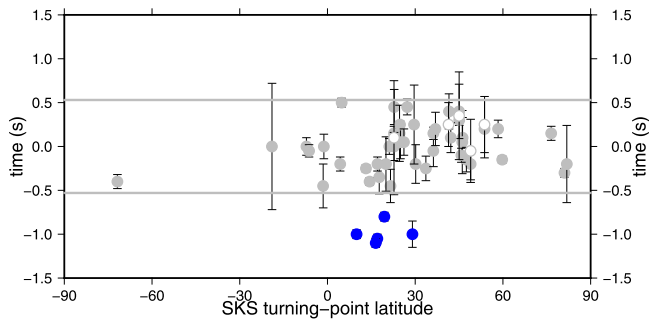


**Fig. 2 Double differential travel times from earthquake pairs.** The smallest differential arrival time change between SKS and reference phases Pdiff, Sdiff, PP, or SS,  $\delta t_{\text{SKS}} - \delta t_{\text{X}}$  (X: Pdiff, Sdiff, PP, SS) is plotted as a function of the SKS wave turning point latitude. Measurement error bars are determined based on a varying time window analysis. For the COLA seismograms in Fig. 1, the value of the smallest relative time change is  $\delta t_{\text{SKS}} - \delta t_{\text{Sdiff}} = -1.05$  s, and the turning point latitude is 17.08°N. The gray open circles are measurements from two earthquakes that are less than 10 years apart in time. The 1.5 standard deviation of  $\delta t_{\text{SKS}} - \delta t_{\text{X}}$  of the dataset is 0.53 s, and it is plotted for reference only. The five anomalous SKS travel times that can not be explained by earthquake mislocations based on hypocenter grid search (Methods) are plotted in blue circles. Except for the SKS waves recorded at station CCM which has a turning point latitude of 29.05°N, the other four anomalous SKS waves are from the same earthquake pair with turning point latitudes at 9.96°N (ULN), 16.51°N (YAK), 17.08°N (COLA), and 19.46°N (INK). The smallest relative arrival time change does not carry significance in analysis but for illustration purposes only.

broader. The same diffraction effects are not observed on the recorded seismograms. The synthetic SKS wave seismograms associated with the larger anomaly that is comparable to the size of the Fresnel zone agree much better with what is observed on the recorded SKS waveforms. We conclude that, while the regions with temporal changes in outer core properties are localized because SKS advance was only observed on a limited number of ray paths, the size of the anomaly may not be much smaller than the size of the Fresnel zone. The observed differential travel time is slightly smaller than that calculated for the large anomaly in Fig. 5. We vary the size and magnitude of the P-wavespeed perturbations of the anomaly and synthetic seismograms calculated using the Spectral Element Method show that a P-wavespeed increase of 1–1.5% in a region with a lateral radius of about 12° (~800 km) and a depth extent of ~800 km in the upper outer core can reasonably explain the observed SKS wave advance times as well as their waveforms. There is some trade-off between the size and the strength of the anomaly. The size of the anomaly may be slightly larger if the anomaly is weaker, but its lateral extent is limited as measurable SKS advance is not recorded on neighboring SKS rays (Fig. 4).

It is worth noting that SKS travel time differences due to ray path sampling different regions of the mantle are negligible for this dataset. This is because the two earthquakes have close hypocenter locations and their SKS ray path separation is much smaller than the size of the Fresnel zones at those periods. Fig. S4 shows SKS ray paths at station ULN for earthquake pair P16 (as in Figs. 5, 6). The largest ray path separation in the mantle occurs at the CMB, where the two rays are about 6 km (0.1°) away from each other, while the radius of the Fresnel zone is about 700 km at the CMB. Therefore, the two SKS waves sample almost the same region of the mantle (circles in Fig. S4). To illustrate the order of magnitude of possible SKS time shifts caused by possible differences in ray path and mantle heterogeneities, we calculate synthetic seismograms in 3D models with a wavespeed anomaly

located at two different positions—one along the ray path and one off the ray path. The SPEC-FEM calculations show that (1) SKS travel time can be affected by anomalies completely off the ray path because what the seismic wave “sees” is the entire structure in the Fresnel zones; and (2) a small change in the relative position between the ray path and the anomaly (1.0° at CMB) does not introduce a measurable difference in the SKS travel time (<0.1 s). For the dataset used in this study, ray path changes associated with earthquake location differences are about 0.1° at the CMB, which is ten times smaller than the example in Fig. S4. The results are consistent with SPEC-FEM simulations in a global mantle wavespeed model S40RTS<sup>10</sup> in which the differential travel time  $\delta t_{\text{SKS}} - \delta t_{\text{Sdiff}}$  due to mantle heterogeneities is essentially zero (Methods).

## Discussion

The exact mechanisms responsible for the 1–1.5% increase in P-wavespeed in localized regions in the outer core over a period of two decades is unclear. It is unlikely that the increase in seismic wavespeed is dominantly a result of temperature change because sound speed is nearly independent of temperature in liquid iron at core pressures<sup>11</sup> and it would require an unreasonably large temperature drop (in the order of 1000 K) in a small region, assuming a temperature derivative  $|d \ln V / dT|$  of about  $10^{-5} / \text{K}$ <sup>12</sup>. The bulk modulus is relatively insensitive to the light elements<sup>11</sup> and the 1–1.5% of velocity increase can be more readily explained as a 2–3% of density deficit due to the high concentration of light elements. For example, if local flows in the outer core contain 1–2 wt% more sulfur<sup>13</sup>. Geodynamo simulations with thermochemical flows in the outer core have shown that cyclonic circulations may cause local high rates of light element release<sup>14</sup>.

The existence of light elements in the outer core has been long understood and global earth models based on seismological observations require some density deficit in the outer core<sup>11,12,15</sup>. The process that light elements are released from the inner core and how they participate in outer core convection are very important for the understanding of the Earth’s geodynamo. If light elements are released from the bottom of the outer core where iron freezes into the solid inner core, the chemical buoyancy associated with light elements will contribute to driving core convection. If the process is not homogeneous, regions with high concentration of light elements will have faster seismic wavespeed. If we assume this observed temporal change in seismic wavespeed reflects upward flows carrying high-concentration light elements, a rough estimate of the distance traveled in the order of 800 km over 20 years would predict a flow speed in the order of 40 km/year, which largely agrees with flow speeds in self-consistent geodynamo simulations<sup>16,17</sup>. However, the actual flow speed might be greater if the process occurred in a shorter time interval between the two earthquake occurrences. The regions with anomalous SKS travel times all occur in the low latitude of the Pacific Ocean and convective core flows that carry high-concentration light elements into this region remain to be understood.

Lateral variations in density associated with large-scale fluid dynamical processes in the outer core are expected to be small<sup>18</sup>. For example, in thermal convections, order of magnitude analysis shows that lateral variations in  $\delta \rho / \rho$  are expected to be smaller than  $10^{-8}$ . The upper limit may be relaxed to  $10^{-6}$  in a stably stratified layer but shear instability would limit density perturbation to  $10^{-4}$ . Even the shear instability can be avoided, any perturbations larger than  $10^{-3}$  (0.1%) would be transient unless there is some efficient process for re-establishing the density contrast<sup>18</sup>. Nevertheless, lateral wavespeed heterogeneities

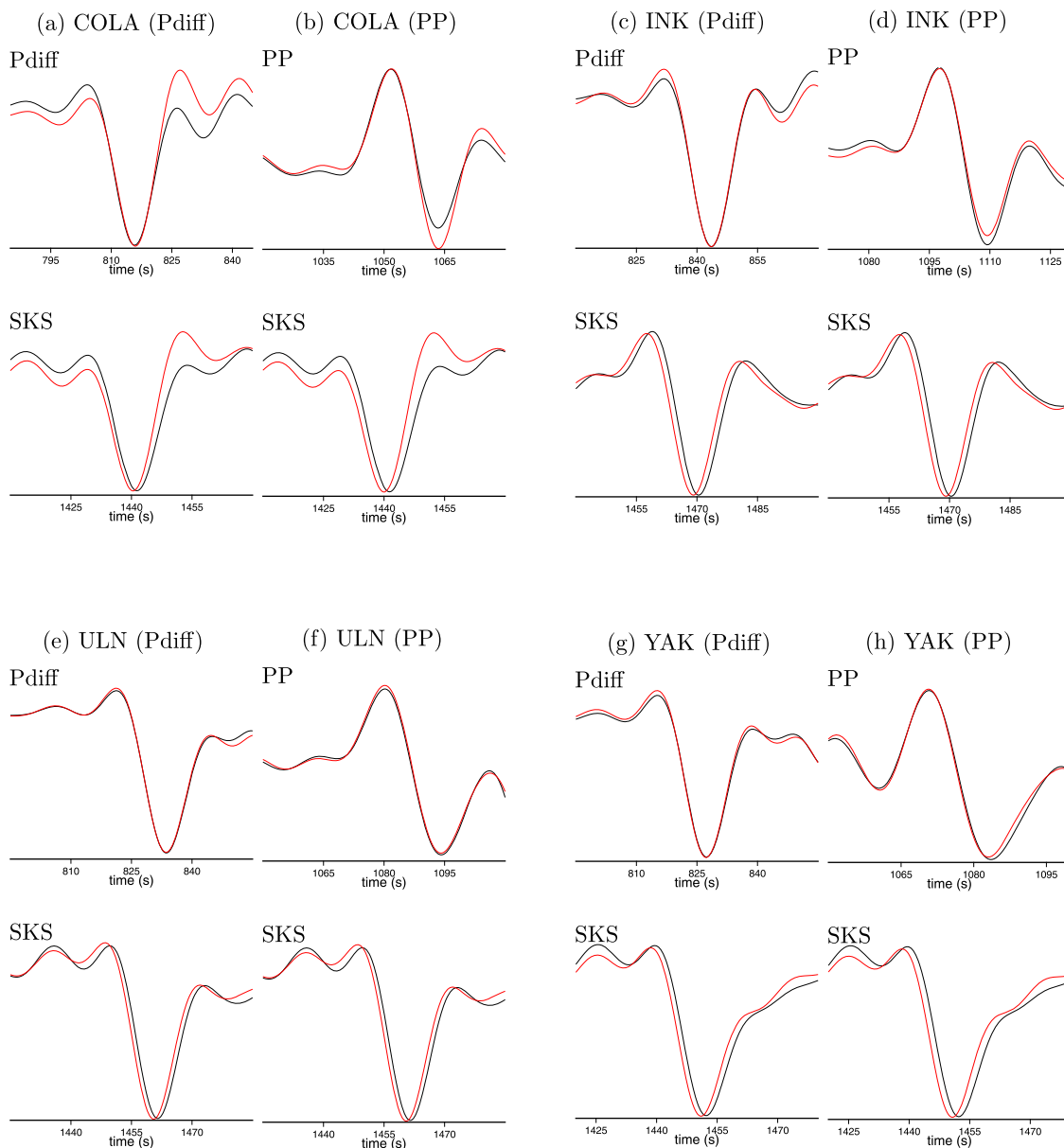


**Fig. 3 Early arrivals of SKS waves from the second earthquake. a–h** Seismograms showing the early arrivals of the core-penetrating SKS waves from the second earthquake when PP and Pdiff waves from the earthquake pair (P16) are aligned. The differential travel times between PP and Pdiff waves are small, with  $\delta t_{PP} - \delta t_{Pdiff}$  being 0.4 s at COLA, 0.1 s at INK, 0.1 s at ULN, and 0.35 s at YAK. This indicates that their distances to the two earthquake epicenters are very close.

exceeding 0.5% in the outer core have been reported at a global scale to improve the data fit of the core-penetrating seismic phases<sup>4,19</sup>. We point out that the temporal perturbation of 1–1.5% in wavespeed observed in this study is not a general feature of the dataset but it is absent in the majority of the measurements. This likely indicates a transient process in the outer core at a decade time scale or shorter, possibly associated with turbulence flows similar to the compositional plumes and blobs originated from the boundary layer at the inner core<sup>20</sup>.

While we interpret the observed temporal changes in seismic wavespeed as density perturbations, other possibilities should also be explored in future studies. For example, possible contributions from regional thermal convection in the outer core controlled by heterogeneities in the lowermost mantle<sup>21</sup> as well as possible descending flows with a considerable amount of suspended solid, which may satisfy the general density limit but introduce differences in bulk modulus and therefore different wavespeed<sup>18</sup>. The

existence of a stratified layer at the top of the outer core has been investigated in recent studies<sup>22–27</sup>. If the observed temporal change in the SKS arrival times comes from a thin layer (60–300 km) at the top of the outer core, it would require large P-wavespeed perturbations (3–15%) even for anomalies with lateral sizes exceeding the size of the Fresnel zone. Rapid temporal changes in core flows with such strong perturbations are probably least expected in a stably stratified layer. While the connection between the wavespeed change observed in this study and the formation of a possibly stratified layer at the top of the outer core remains unclear, simulations of chemical plumes and blobs indicate that the possibility of building a stratified layer by an accumulation of light chemical plumes and blobs may not be excluded<sup>20</sup>.

The latent heat and chemical buoyancy associated with the growth of the inner core drive convections in the outer core. The process is probably not uniform as hemispherical differences in inner core structure have been reported<sup>28</sup> and complex core



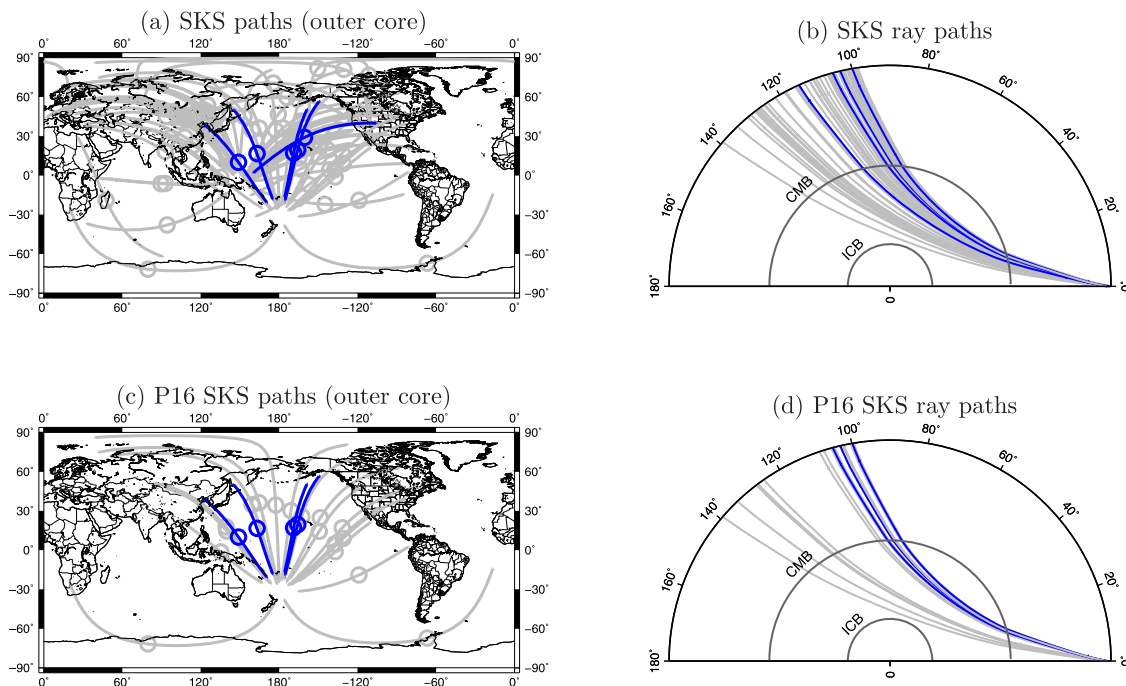


**Fig. 4 SKS ray paths in map view and cross-section view.** **a** SKS great-circle ray path segments in the outer core for the entire dataset. The circles indicate the turning points of the SKS waves. The blue paths are the anomalous SKS waves that can not be explained by possible earthquake mislocations. The cross-section view of the SKS paths are plotted in **(b)**, the anomalous SKS paths all turn in the upper half of the outer core. **c, d** are the same as **(a)** and **(b)** but for earthquake pair P16. CMB Core-Mantle boundary, ICB inner core boundary.

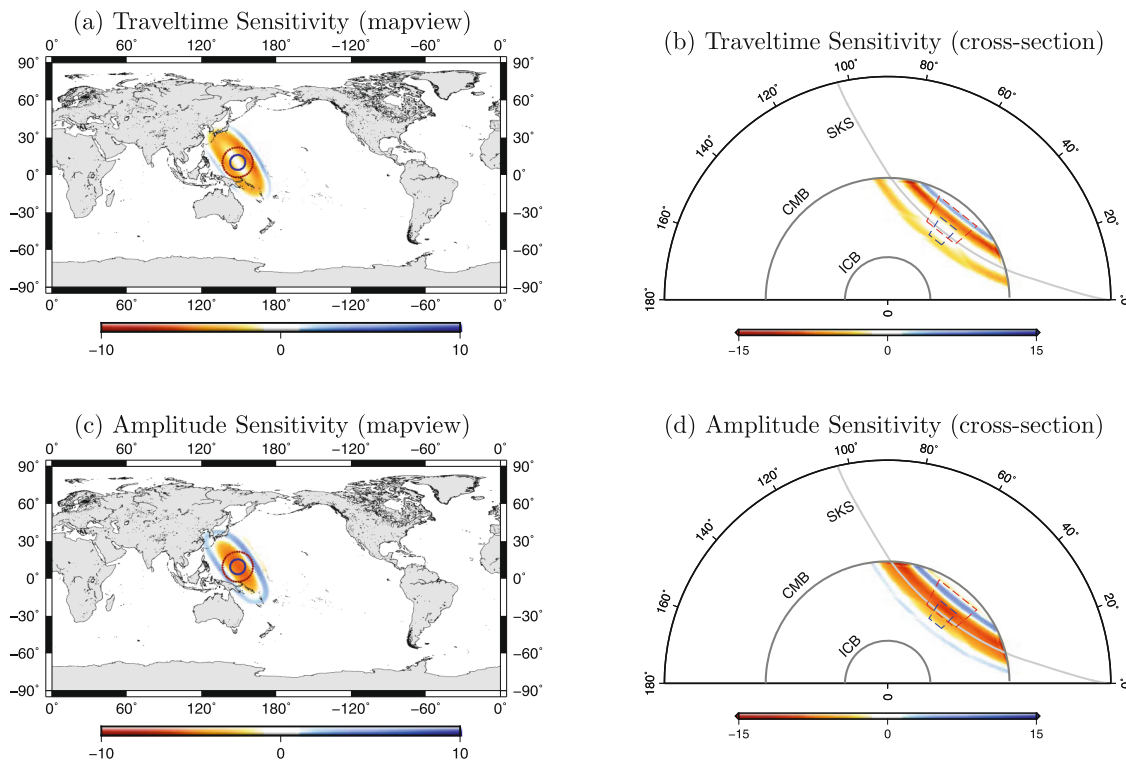


**Fig. 5 SKS finite-frequency sensitivity and outer core anomalies used in modeling.** **a** and **b** are map view and cross-section view of the SKS travel time finite-frequency sensitivity at a period of 30 s, calculated for the SKS wave at station ULN (turning point latitude 9.96°N). The map views are plotted at the turning depth of the SKS wave. **c** and **d** are the same as **(a)** and **(b)** but for the amplitude of the SKS wave. The wavespeed anomalies used in Fig. 6 are also plotted here for reference. The anomalies are axis symmetrical with a cylindrical (conical) shape. The small anomaly (blue) has a radius of 6° and a depth extent of 600 km centered on the ray path. The large anomaly (red) has a radius of 12° and a depth extent of 800 km above the geometrical ray.

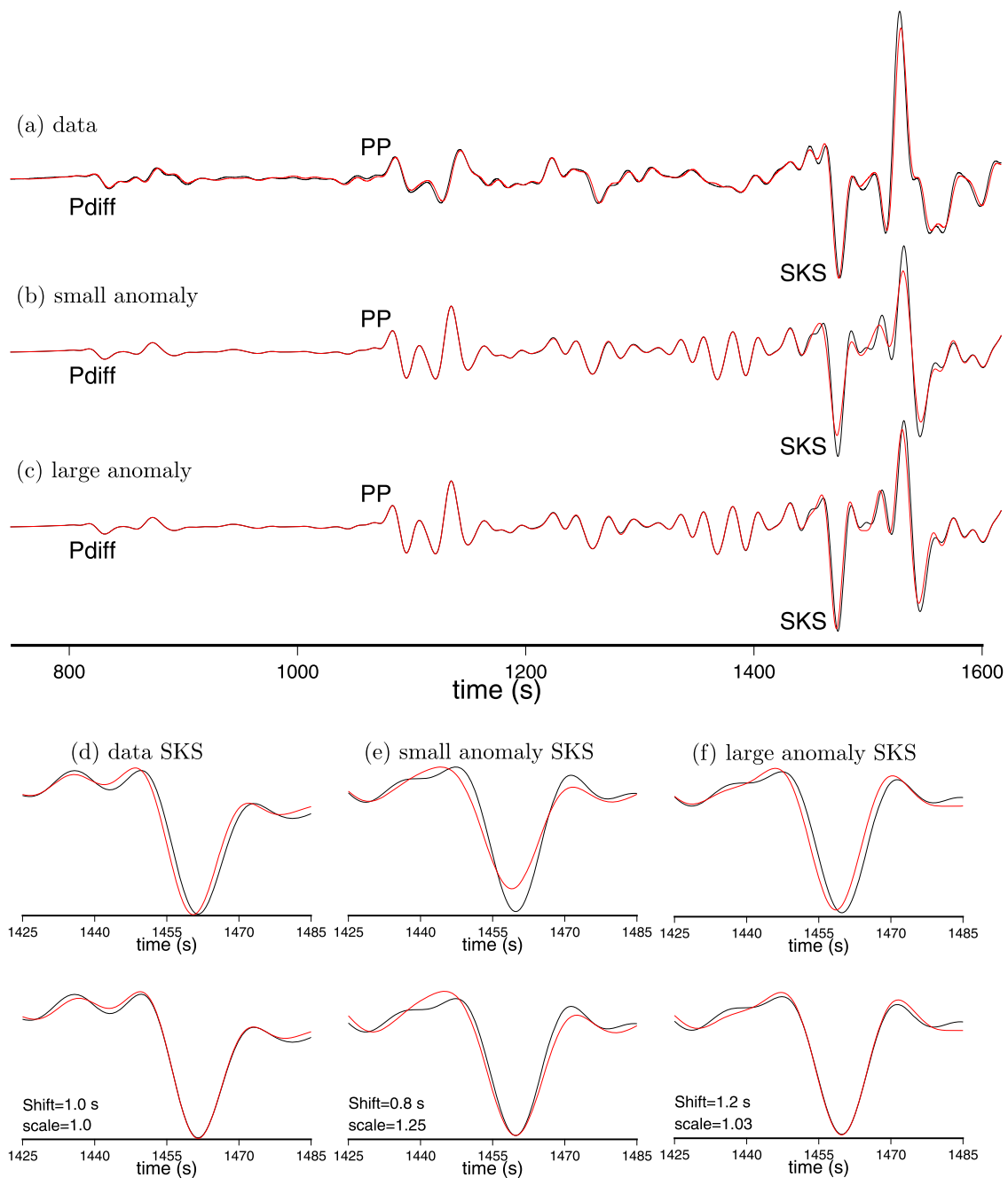


**Fig. 6** SPECfEM seismograms calculated for different size core anomalies. **a** Observed seismograms at station ULN. A longer section of the original seismograms are plotted in Fig. S5. The SKS wave travels faster at the time of the second earthquake (red line). **b** and **c** are synthetic seismograms calculated for a small and a large anomaly in the outer core. **d-f** are zoom-in views of the SKS waves. The small anomaly has a radius of  $6^\circ$  and P-wavespeed increase of 4%; and the large anomaly has a radius of  $12^\circ$  and P-wavespeed increase of 1.5%, respectively. The locations of the anomalies are plotted in Fig. 5. The reference 1D model is PREM. It is worth noting that the observed data in **(a)** are for two different earthquakes with different focal depths, and therefore their depth phases have different arrivals. The synthetics in **(b)** and **(c)** are for two identical earthquakes, with the only difference being the P-wavespeed perturbations in the outer core. The purpose of this figure is to illustrate the effects of wave diffraction on SKS waveforms, not to model the complete seismograms from the two earthquakes which also depend on mantle structure. While a strong small anomaly and a large weak anomaly may produce the same amount of time shift on the SKS wave, the small anomaly introduces strong wave diffraction effects which result in smaller amplitude and broader waveform of the SKS wave.

growth models have been proposed<sup>29</sup>. While the convection in the liquid outer core has a much shorter time scale than the convection in the mantle, observations in this study show that the outer core is far from well mixed in a decade time scale, and, lateral heterogeneities associated with outer core convection are strong enough to produce seismic wavespeed changes detectable

in earthquake recordings. This opens the possibility of monitoring temporal changes in the outer core using seismic data.

### Methods

**Data selection and processing.** We use large earthquakes between 1990 and 2019 in the USGS PDE catalog with event magnitudes greater than 6.0. We search for

pairs of earthquakes that occurred in different decades and their epicenter locations are less than 100 km away from each other. This returns 21 earthquake pairs (Table S1). We exclude two earthquake pairs that have focal depth differences greater than 35 km. For each earthquake pair, we requested available three-component broadband displacement seismograms at FDSN stations that have epicentral distances between 98° and 145°. Instrument responses are removed and horizontal seismograms are rotated to radial and transverse components. The seismograms are band-pass filtered between 20 and 100 s period using a zero-phase Butterworth filter. We visually inspect the quality and similarity between seismograms for every earthquake pair, and events that are affected by large foreshocks or have different source radiations are removed. Seismograms with low signal-to-noise ratios are discarded. This leaves a total of seven earthquake pairs from which 55 high-quality SKS measurements are made. The majority (50) of the SKS measurements are from six earthquake pairs that have a first earthquake occurred in the 1990s and the second one occurred in the 2010s.

**Differential travel time measurements.** We measure the relative travel times using seismograms from each earthquake pair based on cross-correlation. The measurements are made for the following phases: SKS, Pdiff, Sdiff, PP, and SS. SmKS waves are not used due to possible interference with depth phases. The relative arrival times  $\delta t_{\text{SKS}}$ ,  $\delta t_{\text{Pdiff}}$ ,  $\delta t_{\text{Sdiff}}$ ,  $\delta t_{\text{PP}}$ , and  $\delta t_{\text{SS}}$  are then used to find the differential travel times  $\delta t_{\text{SKS}} - \delta t_{\text{X}}$  (X: Pdiff, Sdiff, PP, or SS). The double differential travel times minimize uncertainties associated with source origin times and possible clock errors<sup>30</sup>. Not all seismograms have clear arrivals of all reference phases, but every measurement set includes at least one reference P wave (Pdiff or PP) and one reference S wave (Sdiff or SS) measurement. We estimate measurement error bars using the standard deviation of measurements made with varying time windows by moving the start time and the end time of the measurement window up to 10 s at a 1-s time interval (Fig. S6). The smallest values of  $\delta t_{\text{SKS}} - \delta t_{\text{X}}$  from each measurement set and the SKS measurement error bars are plotted in Fig. 2.

**Uncertainty estimates and hypocenter grid search.** To estimate uncertainties in differential travel times associated with mantle heterogeneities, we calculate seismograms for earthquake pairs in a 3D wavespeed model S40RTS<sup>10</sup> and differential travel time measurements made on synthetic seismograms show that  $\delta t_{\text{SKS}} - \delta t_{\text{X}}$  are all less than 0.3 s. In addition, the differential travel times  $\delta t_{\text{SKS}} - \delta t_{\text{Sdiff}}$  due to mantle heterogeneities are minimum (zero). In this study, we use 0.5 s as the maximum uncertainty to determine if observed differential measurements may be explained by possible earthquake hypocenter mislocations (Fig. S6). We perform a grid search of an alternative hypocenter for each earthquake in a spherical region with a radius of 50 km, centered at the USGS PDE locations and an example is illustrated in Fig. S8. We calculate  $\delta t_{\text{SKS}} - \delta t_{\text{X}}$  (X: Pdiff, Sdiff, PP, or SS) for each alternative hypocenter location and compare the calculations with observed values. If the smallest absolute value of  $\delta t_{\text{SKS}} - \delta t_{\text{X}}$  as well as  $\delta t_{\text{PP}} - \delta t_{\text{SS}}$  or  $\delta t_{\text{SS}} - \delta t_{\text{Sdiff}}$  are close to the observed data to within  $\pm 0.5$  s, we conclude that temporal changes in core properties are not necessary to explain the differential travel times. Using this criteria, we found the majority of the measurement sets may be explained by possible hypocenter mislocations except for five anomalous measurement sets in which the smallest value of  $\delta t_{\text{SKS}} - \delta t_{\text{X}}$  varies between 0.8 and 1.1 s, and, extending hypocenter search radius to 200 km does not change the conclusion. In addition, all SKS waves in the anomalous measurement sets arrive about one second earlier than all other reference phases (Table S2), indicating an increase in P-wavespeed in the outer core at the occurrence time of the second earthquake.

**SPECFEM simulations and finite-frequency sensitivity.** To estimate the size of the seismic wavespeed anomalies in the outer core, we calculate the finite-frequency sensitivity of SKS travel time and amplitude at station ULN (turning latitude 9.96°N) using the SPECFEM adjoint method<sup>6</sup>. The lateral size (radius) of the Fresnel zone is about 800 km at the turning depth of the SKS wave at a period of 30 s (Fig. 4). We calculate synthetic seismograms using the Spectral Element Method<sup>9</sup> for P-wave anomalies with different sizes (from 300 to 1200 km) as well as different perturbation magnitude (1–4%) to investigate wave diffractive effects on the SKS waveforms. The calculations show that anomalies with a 1–1.5% increase in P-wavespeed and a lateral radius of about 800 km can best explain the observed anomalous SKS waves.

## Data availability

Seismic Data used in this research are available from the IRIS Data Management Center (<https://ds.iris.edu/ds/nodes/dmc/data/>).

## Code availability

SPECFEM3D code for wave propagation simulations is available for download from Computational Infrastructure for Geodynamics (CIG) (<https://geodynamics.org>). The GMT software package used to prepare Figures is available at <https://www.soest.hawaii.edu/gmt/>.

Received: 18 October 2021; Accepted: 5 April 2022;

Published online: 25 April 2022

## References

- Birch, F. Elasticity and constitution of the earth's interior. *J. Geophys. Res.* **57**, 227–286 (1952).
- Stevenson, D. J. Models of the earth's core. *Science* **214**, 611–619 (1981).
- Wood, B., Walter, M. & Wade, J. Accretion of the earth and segregation of its core. *Nature* **441**, 825–833 (2006).
- Vasco, D. W. & Johnson, L. R. Whole earth structure estimated from seismic arrival times. *J. Geophys. Res.* **103**, 2633–2671 (1998).
- Soldati, G., Boschi, L. & Piersanti, A. Outer core density heterogeneity and the discrepancy between PKP and PcP travel time observations. *Geophys. Res. Lett.* **30**, 1190 (2003).
- Tromp, J., Tape, C. & Liu, Q. Seismic tomography, adjoint methods, time reversal and banana-doughnut kernels. *Geophys. J. Int.* **160**, 195–216 (2005).
- Dahlen, F. A., Hung, S.-H. & Nolet, G. Frechet kernels for finite-frequency traveltimes-i. theory. *Geophys. J. Int.* **141**, 157–174 (2002).
- Dahlen, F. A. & Baig, A. M. Frechet kernels for body-wave amplitudes. *Geophys. J. Int.* **150**, 440–466 (2002).
- Komatitsch, D. & Tromp, J. Spectral-element simulations of global seismic wave propagation - i. validation. *Geophys. J. Int.* **149**, 390–412 (2002).
- Ritsema, J., Deuss, A., van Heijst, H. & Woodhouse, J. S40RTS: a degree-40 shear-velocity model for the mantle from new rayleigh wave dispersion, teleseismic traveltimes and normal-mode splitting function measurements. *Geophys. J. Int.* **184**, 1223–1236 (2011).
- Anderson, W. W. & Ahrens, T. J. An equation of state for liquid iron and implications for the earth's core. *J. Geophys. Res.* **99**, 4273–4284 (1994).
- Vocadlo, L. *Treatise on Geophysics* 2nd edn (Elsevier, 2015).
- Anderson, O. L. The gruneisen parameter for iron at outer core conditions and the resulting conductive heat and power in the core. *Phys. Earth Planet. Inter.* **109**, 179–197 (1998).
- Aubert, J., Hagay, A., Hulot, G. & Olson, P. Thermochemical flows couple the earth's inner core growth to mantle heterogeneity. *Nature* **454**, 758–761 (2008).
- Dziewonski, A. & Anderson, D. Preliminary reference Earth model. *Phys. Earth Planet. Inter.* **25**, 297–356 (1981).
- Glatzmaier, G. A. & Roberts, P. H. A three-dimensional convective dynamo solution with rotating and finitely conducting inner core and mantle. *Phys. Earth Planet. Inter.* **91**, 63–75 (1995).
- Christensen, U. R. & Aubert, J. Scaling properties of convection-driven dynamos in rotating spherical shells and application to planetary magnetic fields. *Geophys. J. Int.* **166**, 97–114 (2006).
- Stevenson, D. J. Limits on lateral density and velocity variations in the earth's outer core. *Geophys. J. R. Astr. Soc.* **88**, 311–319 (1987).
- Boschi, L. & Dziewonski, A. M. Whole earth tomography from delay times of P, PcP and PKP phases: lateral heterogeneities in the outer core or radial anisotropy in the mantle? *J. Geophys. Res.* **103**, 2633–2671 (1998).
- Bouffard, M., Choblet, G., Labrosse, S. & Wicht, J. Chemical convection and stratification in the earth's outer core. *Front. Earth Sci.* <https://doi.org/10.3389/feart.2019.00099> (2019).
- Mound, J. E. & Davies, C. J. Scaling laws for regional stratification at the top of earth's core. *Geophys. Res. Lett.* **47**, (2020).
- Alexandrakis, C. & Eaton, D. W. Precise seismic-wave velocity atop earth's core: no evidence for outer-core stratification. *Phys. Earth Planet. Inter.* **180**, 59–65 (2010).
- Helfrich, G. & Kaneshima, S. Outer-core compositional stratification from observed core wave speed profiles. *Nature* **468**, 807–810 (2010).
- Helfrich, G. & Kaneshima, S. Causes and consequences of outer core stratification. *Phys. Earth Planet. Inter.* **223**, 2–7 (2013).
- Olson, P., Landeau, M. & Reynolds, E. Dynamo tests for stratification below the core-mantle boundary. *Phys. Earth Planet. Inter.* **271**, 1–18 (2017).
- Irving, J. C., Cottaar, S. & Lekic, V. Seismically determined elastic parameters for earth's outer core. *Sci. Adv.* **4**, eaar2538 (2018).
- van Tent, R., Deuss, A., Kaneshima, S. & Thomas, C. The signal of outermost-core stratification in body-wave and normal-mode data. *Geophys. J. Int.* **223**, 1338–1354 (2020).
- Niu, F. L. & Wen, L. X. Hemispherical variations in seismic velocity at the top of the earth's inner core. *Nature* **410**, 1081–1084 (2001).
- Monnereau, M., Calvet, M., Margerin, L. & Souriau, A. Lopsided growth of earth's inner core. *Science* **328**, 1014–1017 (2010).
- Yang, Y. & Song, X. Temporal changes of the inner core from globally distributed repeating earthquakes. *J. Geophys. Res.* **125**, e2019JB018652 (2020).



## Acknowledgements

This research was supported by the US National Science Foundation under Grant EAR-2017218. The author acknowledges Advanced Research Computing at Virginia Tech for providing computational resources and technical support.

## Author contributions

The sole author of this work, Y.Z., conducted the study in its entirety.

## Competing interests

The authors declare no competing interests.

## Additional information

**Supplementary information** The online version contains supplementary material available at <https://doi.org/10.1038/s43247-022-00432-7>.

**Correspondence** and requests for materials should be addressed to Ying Zhou.

**Peer review information** *Communications Earth & Environment* thanks the anonymous reviewers for their contribution to the peer review of this work. Primary Handling Editors: Claire Nichols, Joe Aslin, and Clare Davis. Peer reviewer reports are available.

**Reprints and permission information** is available at <http://www.nature.com/reprints>

**Publisher's note** Springer Nature remains neutral with regard to jurisdictional claims in published maps and institutional affiliations.



**Open Access** This article is licensed under a Creative Commons Attribution 4.0 International License, which permits use, sharing, adaptation, distribution and reproduction in any medium or format, as long as you give appropriate credit to the original author(s) and the source, provide a link to the Creative Commons license, and indicate if changes were made. The images or other third party material in this article are included in the article's Creative Commons license, unless indicated otherwise in a credit line to the material. If material is not included in the article's Creative Commons license and your intended use is not permitted by statutory regulation or exceeds the permitted use, you will need to obtain permission directly from the copyright holder. To view a copy of this license, visit <http://creativecommons.org/licenses/by/4.0/>.

© The Author(s) 2022